Fundamentals of High Temperature Processes

Effect of initial total concentration on the rate of SiO₂ inclusion removal from molten Cu
K.OKUMURA et al.

The effect of initial total oxygen concentration, $[\text{mass}\%O]_{T0}$, on the rate of inclusion removal from molten copper has been investigated.

Under the mechanical stirring condition, it is found that the rate constant of inclusion removal, K_o, is dependent on $[\text{mass}\%O]_{T0}$ and almost independent of the rotation speed of stirrer. From the results of microscopic observation of inclusion particles with SEM, size distribution of inclusion particles is obtained. The rate constant, K_o, increases with increasing initial value of number density and mean radius of inclusion particles. Agglomeration of inclusion particles affects the rate of inclusion removal.

Under Ar gas injection stirring condition, K_o, increases with increasing gas flow rate, while it does not apparently depend on $[\text{mass}\%O]_{T0}$, and the effect of the agglomeration on the rate of inclusion removal is much smaller than that under the mechanical stirring condition. It is considered that the inclusion particles are removed from the melt mainly through adhesion to the gas bubble-metal interface.

Prediction of the optimum bubble size for inclusion removal from molten steel by flotation
L.WANG et al.

A mathematical model has been developed to determine the optimum bubble size for the removal of inclusions from molten metals by flotation. The probability of collision between a bubble and an inclusion, P_C, and the probability of adhesion of an inclusion to a bubble by sliding, P_A, are defined to describe the efficiency of inclusion attachment to a bubble. The results show that small bubbles have a high P_C, while small inclusions have a high P_A and low P_C. By considering the overall probability, $P(=P_C \times P_A)$, and the floating time of the bubble, the model suggests that the optimum bubble sizes for the removal from steel of alumina inclusions less than 50 μm in size are in the range of 0.5 to 2 mm in diameter.

Molten steel refining using fine gas bubbles
L.WANG et al.

A new process has been developed for metal refining. This process involves the creation and dispersion of fine bubbles in molten metals by introducing inert or reactive gas into a turbulent flow region during metal transfer. The highly turbulent metal flow splits the gas into fine bubbles and results in good mixing between the gas and molten metal phases. These conditions are ideal for contacting inclusions in the metal with the bubbles and subse-quent flotation of the inclusions to the metal-slag interface where the inclusions are then absorbed by the covering slag layer. Dissolved gases, such as [H], [O], [N], in the metals are also transferred to the gas bubbles and removed from solution. The process can be retrofitted into existing process plants.

The process concept has been demonstrated using a full-scale air/water model to simulate the ladle-to-tundish system of continuous casting of steel. At liquid flows typical of those encountered in the caster, fine bubbles smaller than 0.5 mm in diameter can be created and a good mixing between the dispersed gas and the liquid has been achieved.

Thermodynamics of the nickel-aluminum-oxygen and nickel-iron-aluminum-oxygen melts in equilibrium with soid alumina
F.ISHII et al.

The deoxidation equilibrium of aluminum in liquid nickel equilibrated with solid alumina has been measured at the temperature ranges from 1 823 to 1 973 K using the sampling technique in order to investigate the equilibrium between aluminum and oxygen in liquid nickel for the refractory alloy or superalloy.

For the deoxidation reaction in pure liquid nickel, i.e.:
$$Al_2O_3(s) = 2\underline{Al} + 3\underline{O}$$
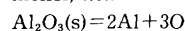
the temperature dependence of the equilibrium constants, $K_{Al}(=a^2_{Al} \cdot a^3_O/a_{Al_2O_3})$, was expressed to be:
$$\log K_{Al} = -28\,770/T + 1.67 \qquad 1\,823-1\,973 \text{ K}$$

while the deoxidation product, $K'_{Al}(=[\%Al]^2 [\%O]^3)$, and the effect of aluminum on the activity coefficient of oxygen in liquid nickel were obtained to be:
$$\log K'_{Al} = \log K_{Al} + 1.47(3[\%Al] + 3.4[\%O])$$
$$\log f_O^{Al} = -1.47[\%Al]$$
$$Al < 1.1 \text{ mass}\%, \ 1\,823-1\,973 \text{ K}$$

The deoxidation equilibrium of aluminum in liquid nickel-iron binary alloys with 0.01-0.1 mass% aluminum has been measured up to 50 mass% iron. The effect of iron on the activity coefficients of oxygen and aluminum in liquid nickel-iron alloys based on pure liquid nickel were estimated as the following expression:
$$\log f_O^{Fe} + 2/3\log f_{Al}^{Fe} = -0.028[\%Fe]$$
up to around 10 mass% iron at 1 923 K.

The effect of nickel on the activity coefficient of aluminum in liquid iron-nickel based on liquid iron were also discussed using $\log K_{Al(Fe)}$ in liquid iron and the present results.

Ironmaking and Reduction

Model studies of liquid flow in the blast furnace lower zone
G.S.GUPTA et al.

The non-wetting flow of liquid iron in the blast furnace lower zone is simulated experimentally using a two dimensional raceway model with water, air and 4.1mm diameter polyethylene beads to represent liquid iron, blast furnace gas and the coke bed respectively. An X-ray technique is used to visualise liquid flow in the packed bed and the distribution of liquid from the bottom of the bed is measured. The liquid percolates through the packed bed as series of rivulets which are continuously breaking up and rejoining. The direction and magnitude of the percolation velocity is determined by the balance between three forces acting on the liquid-gravity, gas drag and bed resistance. The gas drag has a very strong effect on the liquid distribution, forcing the liquid away from the raceway region. This effect increases with increasing gas flow rate. At high gas flow rate, the liquid flow rate and distribution at the top of the bed do not effect the liquid distribution leaving the bed. Near the raceway, the packed bed is dry. The size of the dry region increases with increasing gas flow rate. Above the raceway, beyond the dry packed bed, is a region of high liquid holdup. Liquid dripping into this region has a high residence time compared to liquid falling through the deadman zone. A mathematical model for liquid flow is outlined which gives good agreement with experimentally observed liquid flow patterns in the cold raceway model and could be suitable for predicting the liquid flow pattern under real blast furnace conditions. This study confirms that the effect of gas drag on the flow of liquid iron through the blast furnace lower zone is important and should not be neglected.

Apparent coal viscosity estimated from needle penetration into pellet of pulverized coal particles
K.MATSUOKA et al.

Needle penetration and volumetric dilation were measured for cylindrical pellets of six kinds of pulverized coal particles using a needle penetrometer. The measurements were conducted for a range of the heating rate from 1 to 20K/min, the holding temperature from 698 to 823K and the nitrogen gas pressure from 0.1 to 3.0MPa. Both needle penetration and dilation characteristics depended on these operating variables. Especially, an appreciable needle penetration occurred at high heating rate for coals which exhibited little softening property at low heating rate. Unreasonably high activation energies for viscosity were obtained when the needle penetration curves were analyzed on the basis of an equation of motion assuming that the pellet behaves as a Newtonian fluid with a temperature dependency of viscosity given by Andrade's equation.

Steelmaking and Refining

Steelmaking and industrial ecology-Is steel a green material ? (Review)
J.SZEKELY

After a brief review of the evolution of the steel industry during the past 25 years, some basic definitions are presented, including that of industrial ecology, advanced materials, and "green" materials. Then, we discuss the environmental problems that are inherently associated with both conventional and novel steel processing technologies, touching on pollution control, waste minimization and recycling. The important conclusion is reached that when modern technologies are employed, steel is both an advanced material and a green material. Particularly noteworthy in the finding is that steel is one of the most recycled materials in current use. The paper concludes with the enumeration of the tasks ahead and with the definition of the steelplant of the future, which will have to be clean, environmentally benign, located close to the customer and will produce no waste. Indeed, it may derive significant revenue streams from the treatment of wastes produced by other industrial activities. By its very nature, the future steelplant will have to use some mixture of scrap and virgin iron units. It will be frugal on energy, highly flexible in operation, and will exploit synergies with other industrial systems.

Casting and Solidification

Effect of composition of immersion nozzle on occurrence of blister in steel sheet
K.SASAI et al.

The effect of the inner porous refractories-molten steel reaction on the incidence of blisters and the mechanism whereby the incidence of blisters is prevented by using an immersion nozzle with a silicaless inner porous refractories that does not react with the molten steel were studied. The following results were obtained:
(1)Blisters are caused by 0.5mm and larger argon gas bubbles, and particulary 1.0mm and larger argon gas bubbles have a strong bearing on the incidence of blisters in the sheet product.
(2)The mechanism whereby the incidence of blisters depends on the number of sequence cast heats can be explained by the increase in argon gas bubble diameter caused by the inner porous refractories-molten steel reaction in the later heats in the sequence cast.
(3)Fine argon gas bubbles can be stably injected into the molten steel by using an immersion nozzle with a silicaless inner porous refractories that does not react with the molten steel. This stable injection of fine argon gas bubbles helps prevent the occurrence of blisters in the sheet product.

Physical and mathematical modelling of an extended nozzle for metal delivery to high speed, thin strip casting machines
C.JEFFERIES et al.

Numerical fluid flow predictions were compared with experimental flow measurements and visualization for a water model of a novel thin-strip planar-flow delivery system. The proposed slot-type planar-flow delivery system could contain a porous flow modifier and features an extended-reservoir delivery to the substrate. The experiments were carried out with water in a plexiglass model with and without the presence of ceramic foam filters. Flow visualization and velocity measurements downstream from the filter zone showed that the latter had beneficial effects in suppressing the recirculatory flow and supplying fluid of uniform velocity to the substrate. A steady, two-dimensional fluid dynamics model was developed to predict and supplement the experimental studies. This numerical model is based on the use of the Brinkman-Forchheimer extended-Darcy model in the porous filter medium and the Navier-Stokes equation in the fluid region. These two flows are coupled through the interface boundary conditions at the porous-media-fluid interface. Solutions of the coupled governing equations for the complex media and fluid regions were performed using a control-volume, finite-difference technique. The results were grid independent and converged within 2000 iterations and 30 minutes on an IBM 486. Comparison of measured fluid velocities at representative locations downstream of the filter zone showed good agreement with predicted velocities.

Microstructure

Age hardening in a Cu-bearing high strength low alloy steel
S.S.G.BANADKOUKI et al.

The copper age hardening response in a low alloy variant of the ASTM A710 type steel has been investigated at temperatures of 450, 500, and 550 °C for three pre-treated conditions (as rolled ferrite, bainitic ferrite, and martensite). Transmission electron microscopy has been used to follow microstructural changes and their relation to the variations in the hardness curves. The results indicate that the age hardening responses of both the martensitic and bainitic ferrite structures are much higher than that of the as rolled condition, and this observation is rationalised in terms of higher solute Cu content, higher density of dislocations and greater uniformity of solute copper atoms in the pre-treated condition providing a multitude of nucleating sites for copper precipitation. Moreover, it has been found that the peak hardness in the martensitic and bainitic structures was attained when fine ε-copper precipitates are predominantly observed on dislocations. Compared to the martensitic and bainitic structures, the presence of pre-existing inter-phase ε-copper precipitates, as well as the formation of additional copper-rich clusters and precipitates from supersaturated ferrite contribute to the aging response in the hot rolled condition.

Effect of finishing temperature on hot band textures in an IF steel
M.P.BUTRON-GUILLEN et al.

The effect of hot rolling parameters on texture development was studied in a 0.004%C-0.02%Nb-0.02%Ti interstitial free (IF) steel. Two austenitizing temperatures (1250°C or 1150°C) and two levels of reduction (90% or 75%) were employed. Six different finishing temperatures were investigated: 1020°C, 920°C, 870°C, 820°C, 720°C, and 620°C. The final ferrite textures were measured; these are presented in the form of $\varphi_2 = 45°$ ODF sections and of intensities along the RD, TD and ND fibres. The experimental textures display two contrasting behaviours, which depend on finishing temperature. The textures corresponding to the three higher finishing temperatures are relatively flat, with the rotated cube {001} <110> prevailing. Sharper textures are produced at the three lower temperatures; orientations between {001} - {111} <110> are enhanced, the ND ‖ <111> fibre is strengthened, and orientations around {554} <225> are clearly more intense. The experimental results are compared with predictions based on the Kurdjumov-Sachs relation; the differences observed indicate the occurrence of both variant selection and selective growth during transformation.

Morphology of γ'' precipitates in a Ni-15Cr-8Fe-6Nb alloy
K.KUSABIRAKI et al.

The morphology of γ'' precipitates extracted from a nickel-base superalloy, a modified NCF 3 type alloy (X-750M), was investigated mainly by transmission electron microscopy (TEM). The TEM images using carbon extraction replica of γ'' precipitates were clearer than those using electro-polished thin film. The γ'' precipitates were disc shaped in the early stage of aging and became elliptic or irregular shaped plates in latter at up to 1033K, while they grew in rectangular shaped plates in latter at 1073K. Many of larger γ'' Precipitates in the specimens aged at up to 1033K exhibited a considerable amount of internal fringe contrast. Selected area diffraction pattern from them showed continuous streaks normal to {112} γ''. The internal contrast is thought to be due to stacking faults. The internal fringe contrast was not observed in γ'' precipitates in the specimen aged at 1073K.

Effect of boron on intra-granular ferrite formation in Ti-oxide bearing steels
K. YAMAMOTO et al.

The effect of B on microstructure and toughness at the heat affected zone after welding thermal cycle simulations has been investigated in steels containing titanium oxide particles. The titanium oxide is identified as Ti_2O_3 with cation vacanies, which contribute to preferential nucleation of MnS and TiN precipitates on Ti_2O_3. The Mn-depleted zone is formed around Ti_2O_3 after the precipitation of MnS. The Ti_2O_3 particles with TiN and Mn-depleted zone act as preferential nucleation sites for intra-granular ferrite. The segragation of B at austenite grain boundaries suppresses effectively the nucleation of grain boundary ferrite. Ferrite nucleation at the interface between Ti_2O_3 and austenite matrix is not affected by B addition because of B-depleted zone arisen from the diffusion of segregated B into Ti_2O_3 *via* cation vacancies. Consequently the B addition to steels with Ti_2O_3 promotes the formation of fine intra-granular ferrite grains so that the toughness in heat affected zone is improved even after large heat input welding.

Physical and Mechanical Properties

Comparison of experimentally measured and theoretically predicted erosion rates of steels in slurries of low velocity
S. ENDO et al.

The predominant mechanism of weight loss for various kinds of steels in a low velocity slurry environment was evaluated to determine properties governing their weight loss. Erosion was the main reason of the losses. The predominant erosion mechanism could change depending on the angle of particle impact and hardness of the steels even for the same impact velocity condition. In the case of high angle impact, the erosion rate showed good correlation with the erosion rate calculated by the equation.

$$Er = \frac{L^3 \Delta \varepsilon}{\varepsilon_c}$$

where Er is the erosion rate, and $\Delta \varepsilon$ and ε_c are the strain from each impact and the critical strain needed to cause material detachment, respectively. L is the length of the plastic deformation zone beneath the erosion surface. In the case of low impact angle erosion of lower hardness steels, the dominant mechanism is the same as the mechanism for high angle impact. Judging from the hardness distribution beneath the erosion surface and the erosion rates, the dominant mechanism could be fatigue in low angle impact of higher hardness steels.

Ferrite-martensite dual phase anti-erosion steel
S. ENDO et al.

In a slurry environment, increasing the hardness and the work hardening index of a steel both provide excellent erosion resistance. In order to get a steel with higher hardness and work hardening index, the effect of the volume fraction of martensite on these properties in a ferrite-martensite dual phase steel having a higher work hardening index compared to similar hardness steels with other microstructures was investigated. Using the theory developed by Tomota *et al*, the hardness and the work hardening indices of some ferrite-martensite dual phase steels are calculated. It is shown by the calculation that the steels with 0.2 to 0.7 martensite volume fraction show much higher work hardening indices than other microstructural steels with similar strength. Experimentally, the steel with approximately 0.3 martensite volume fraction shows higher work hardening index and twice as much erosion resistance compared to similar hardness steels without the dual phase microstructure.

Relation between magnetostriction and magnetic domains in different directions of grain oriented silicon steel sheet
H. MASUI et al.

Research has been carried out on the magnetostriction measured in changing direction of grain oriented silicon steel sheets. When the magnetic field is applied in a direction of 45° off the rolling direction normally parallel to Goss texture orientation, the magnetostriction indicated negative value regardless of compressive stress applied to specimen and showed favourably smaller nega-

tive value in poor coating stress condition rather than in good one, which had not been easily imagined by the experience concerning to the magnetostriction in the rolling direction. This was explained by a fact that the 90° supplementary domains by compressive applied stress followed by the strain elastic energy theory, which cause positive magnetostriction when the specimen is exposed to magnetic field, is compensated by negative magnetostriction by the abnormal supplementary domains newly generated under magnetic field. The abnormal supplementary domain occurs in specimen with the angle to the rolling direction of about 30° ~ 60°, which was tried to explain by magnetic domain energy. When the magnetic field is applied in a direction of 90° off the rolling direction, the magnetostriction indicated the largest positive value which had been easily supposed by the reaction of the 180° main domain exposed to magnetic field transversely.

New Materials and New Processes

Cold-rolling and recovery behaviour of Ti₃Al single crystals with DO₁₉ structure
T. NAKANO et al.

Effects of activated slip systems, rolling direction and chemical composition on cold-rolling behaviours were investigated in Ti_3Al single crystals containing 25.0at%Al and 33.0at%Al with the DO_{19} structure. Work-hardening and deformability of Ti_3Al depended strongly on the operative slip systems. When the rolling axis and rolling plane was controlled to operate dominantly prism slip of $\{10\bar{1}0\}$ $\langle 1\bar{2}10 \rangle$, Ti-25.0at%Al single crystals could be cold-rolled to about 60% reduction in thickness accompanied by gradual work hardening. However, activation of slips on (0001) and $\{11\bar{2}1\}$ pyramidal planes induced strong work-hardening resulting in poor ductility. Deformability of Ti_3Al was influenced by chemical composition and the best deformability was obtained at the stoichiometric composition. Annealing after heavy cold-rolling resulted in the occurrence of polygonisation. A Ti_3Al sheet was obtained by a thermo-mechanical process combining cold-rolling with annealing.